Science Bulletin 70 (2025) 1174–1181

Contents lists available at ScienceDirect

Science Bulletin

journal homepage: www.elsevier.com/locate/scib

Article

Tripling of MJO residence time over the rapidly warming Indian Ocean during summer monsoon

Wenjun Zhang [a,*], Xuben Lei [b], Guosen Chen [a], Pang-Chi Hsu [a], Feng Jiang [a], Malte Stuecker [c], Fei-Fei Jin [d], Chao Liu [a]

[a] CIC-FEMD/KLME, State Key Laboratory of Climate System Prediction and Risk Management, Nanjing University of Information Science and Technology, Nanjing 210044, China
[b] College of Water Conservancy and Environmental Engineering, Zhejiang University of Water Resources and Electric Power, Hangzhou 210018, China
[c] Department of Oceanography & International Pacific Research Center (IPRC), School of Ocean and Earth Science and Technology, University of Hawai'i at Mānoa, Honolulu 96822, USA
[d] Department of Atmospheric Sciences, School of Ocean and Earth Science and Technology, University of Hawai'i at Mānoa, Honolulu 96822, USA

ARTICLE INFO

Article history:
Received 13 March 2024
Received in revised form 29 December 2024
Accepted 30 December 2024
Available online 27 January 2025

Keywords:
Madden-Julian Oscillation
Stalling behavior
Global warming
Extreme climate events

ABSTRACT

The Madden-Julian Oscillation (MJO) is the dominant mode of intraseasonal tropical atmospheric variability with far-reaching influences on global weather systems. During boreal winter, the MJO typically exhibits regular eastward propagation, whereas in summer, it displays more complex propagation characteristics, such as frequent stalling over the Indian Ocean. Here we show a threefold increase in the MJO residence time over the Indian Ocean during the Asian summer monsoon in recent four decades. This drastic increase is closely associated with the rapid warming of the Indian Ocean, which contributes to increased extreme climate events across Indian Ocean rim countries. This peculiar warming pattern is projected to persist under anthropogenic warming, potentially facilitating prolonged MJO activity over the Indian Ocean with higher climatic disaster risks in the future.

© 2025 Science China Press. Published by Elsevier B.V. and Science China Press. All rights are reserved, including those for text and data mining, AI training, and similar technologies.

1. Introduction

Accurate medium-to-extended-range predictions from several weeks to months in advance represent one of the major challenges of seamless weather-to-climate forecasting. The Madden-Julian Oscillation (MJO), a planetary-scale tropical atmospheric convective system with intraseasonal oscillations [1], has long been identified as a primary source of predictability on these timescales [2]. While largely confined to the deep tropics, the MJO influences the variability of various weather and climate systems both locally and remotely [3,4], such as tropical cyclone activity [5,6], monsoons [7], and the El Niño-Southern Oscillation (ENSO) [8]. Active MJO events can trigger or modulate extreme weather events, such as flooding, droughts, and heat waves in the Middle East, East Asia, North Africa, the Maritime Continent, and North America, leading to serious environmental and socioeconomic consequences [3,9–13]. The MJO has fairly well-defined seasonality in its propagation characteristics [14]. During winter, the MJO is typically observed as a baroclinic eastward-propagating convective system, whereas the MJO in summer shows more complex propagation characteristics. During summer, when a monsoonal flow carries moisture from the tropical oceans into the Asian continent, the MJO can also propagate meridionally in the Asian monsoon region [15–17] (Fig. 1a). While some studies argue that the northward propagating component during boreal summer (i.e., Boreal Summertime Intraseasonal Oscillation) may be independent of its eastward propagation [14,18–20], other studies attribute the northward propagation to the interaction between the eastward propagation of convection at the equator and the background mean state [15,16,21–24]. In this study, we do not draw a strict distinction between these interpretations and instead adopt the concept of the MJO during summertime.

Previous studies have noted that some summertime MJO events exhibit a prominent tendency to stall, occasionally with unexpectedly prolonged convective activity in specific regions [25,26]. For instance, during summer 2020, an active phase of the MJO persisted over the Indian Ocean for an extraordinarily long period of 59 days in June-July, far exceeding the climatological mean of 16 out of 61 days [27–29]. During boreal winter, the propagation features of the MJO are strongly influenced by the background state,

* Corresponding author.
E-mail address: zhangwj@nuist.edu.cn (W. Zhang).

https://doi.org/10.1016/j.scib.2025.01.043
2095-9273/© 2025 Science China Press. Published by Elsevier B.V. and Science China Press. All rights are reserved, including those for text and data mining, AI training, and similar technologies.

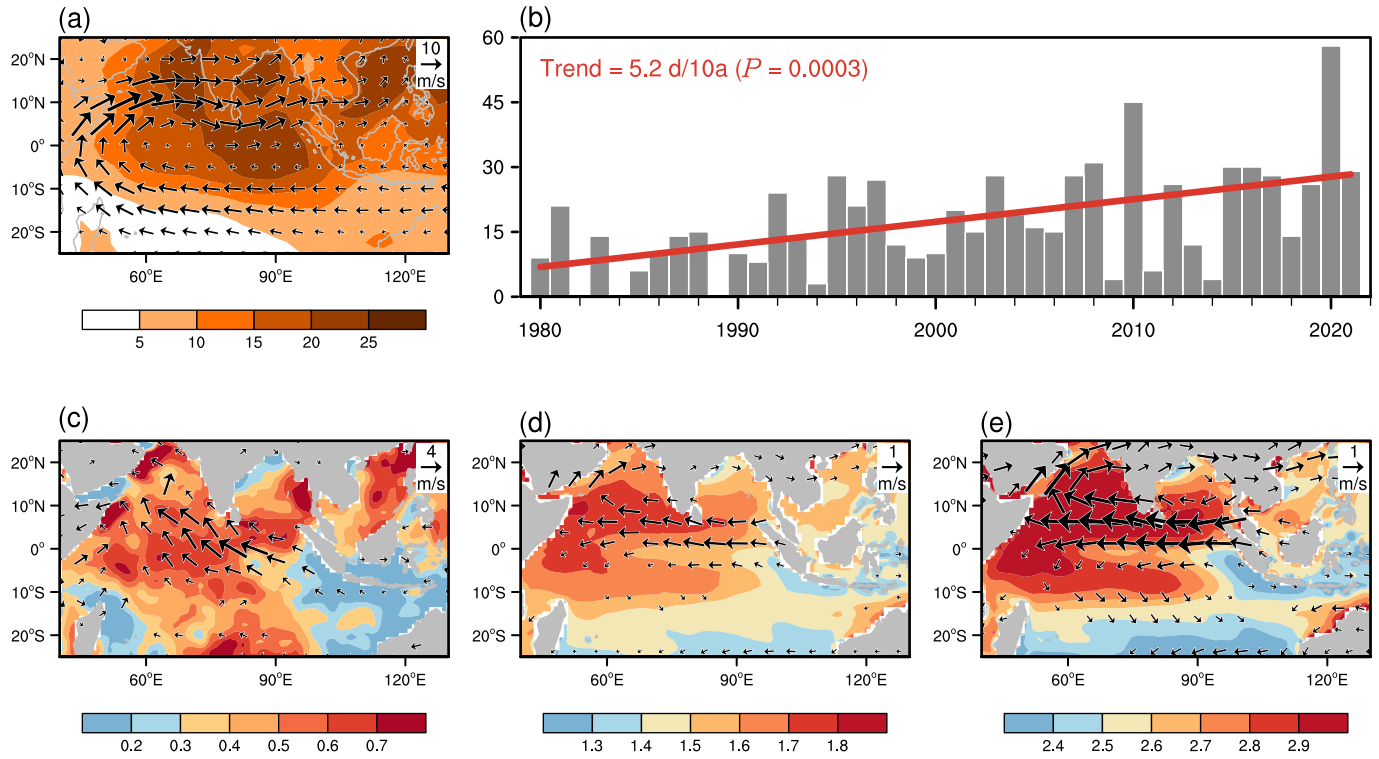


Fig. 1. Long-term trend of MJO residence days in the boreal summer monsoon season and associated background conditions. (a) Standard deviation of intraseasonal (20–90 days) outgoing longwave radiation (OLR) (shading; W/m^2) and climatological mean 850 hPa horizontal wind (vectors; m/s) during June-July of 1980–2021. (b) Time series of MJO residence time (bars; days) in its phase 1 to 3 during June-July season (see Methods). The trend was shown as the thick red line (significant at the 95% confidence level) together with the *P* value. (c) Trends of sea surface temperature (SST; shading; °C per 42 a) and horizontal wind (vectors, m/s per 42 a) during June-July from 1980 to 2021. (d) Differences in SST (shading; °C) and horizontal wind (vectors; m/s) between the last 35 years of SSP2-4.5 scenario (2065–2099) and historical (1980–2014) simulations averaged for 28 coupled models during June-July. (e) Same as (d) but for the SSP5-8.5 scenario.

including sea surface temperature (SST), planetary boundary layer wind, and vertical structure of moisture [30–32]. However, the propagation of the MJO during the Asian summer monsoon, as well as its association with the background air-sea conditions, remains less well understood.

The Indian Ocean, the primary breeding ground of the MJO, has been rapidly warming over recent decades at a rate faster than other tropical ocean basins [33,34], and is projected to warm further in response to anthropogenic greenhouse-gas forcing [35]. Previous work suggests that the residence time of the MJO shows a decreasing trend over the Indian Ocean and an increasing trend over the Maritime Continent-west Pacific during boreal winter along with the expansion of the Indo-Pacific warm pool [10]. Considering the critical role of background atmospheric and oceanic conditions on MJO activity [36], it is reasonable to hypothesize that MJO stalling behavior during the summer monsoon season may have changed in the past and could change further in the future. This issue is highly significant since the increased residence time of MJO over the Indian Ocean during the Asian rainy season increases the likelihood of extreme events in the Indian Ocean rim countries, such as persistent heavy precipitation and severe heat waves, resulting in substantial losses of life and property [28,37]. In this study, we find a threefold rise of the MJO residence time over the Indian Ocean during the Asian summer monsoon season (June-July) over the past four decades. We also address the physical linkages of the increased MJO residence time with the rapid Indian Ocean warming by analyzing the moist static energy (MSE) budget based on observation, reanalysis data and outputs from climate models participating in the Coupled Model Intercomparison Project 6 (CMIP6). This drastic change in the MJO is closely related to a pronounced low-level easterly wind trend, which coincides with rapid warming in the tropical Indian Ocean. The prolonged MJO-related convective activity over the Indian Ocean increasingly contributes to the extreme climate events in the rim countries.

2. Materials and methods

2.1. Definition of the MJO residence time over the Indian Ocean and MSE budget equation

MJO activity was assessed using the Real-time Multivariate MJO (RMM) index [38] from 1980 to 2021, provided by the Australia Bureau of Meteorology. The RMM indices (RMM1 and RMM2), based on the leading two principal components of multivariate Empirical Orthogonal Function analyses of combined daily 850- and 200-hPa zonal wind and outgoing longwave radiation (OLR) anomalies, track the tropical convection on intraseasonal timescales. An active day was defined when the MJO amplitude $((\mathrm{RMM1}^2+\mathrm{RMM2}^2)^{\frac{1}{2}})$ exceeds one. The active days in Phase 1 to 3 summed from 1st June to 31st July were used to characterize the MJO residence time over the tropical Indian Ocean for each boreal summer. Years with long (1995, 1997, 2003, 2007, 2008, 2010, 2015, 2016, 2017, 2020, 2021) and short (1985, 1991, 1994, 2009, 2011, 2014) MJO residence time were identified based on the 3/4 standard deviation above and below the average residence time, respectively (Fig. 1b). It is noted that the years with zero MJO active days (1982, 1984, 1989) are not used for the composites. We adopted an equivalent formulation of RMM indices, that is,

the MJO phase angle ($\varphi = \text{actan}\frac{\text{RMM1}}{\text{RMM2}}$) and the MJO amplitude ($Z = (\text{RMM1}^2 + \text{RMM2}^2)^{\frac{1}{2}}$) to detect possible changes of the MJO.

The MSE budget analysis [25,39] was used to examine the MJO propagation and maintenance mechanism. The MSE is defined as $m = C_pT+Lq+gz$, where C_p represents the specific heat of dry air at constant pressure (1004 J/(K kg), T the temperature, L the latent heat of condensation at 0°C (2.5×10^6 J/kg), q the specific humidity, g the gravitational constant (9.8 m/s^2), and z the geopotential height. The MSE tendency was calculated as the backward difference (with a one-day difference interval) of the MSE before vertically integrating. The MSE tendency is nearly in quadrature with the MSE anomaly, which is usually used to analyze the propagation of the MJO convective anomalies. Composites are generated by averaging all active days for MJO phases 1–3. To examine the propagation characteristics of the MJO, the MSE tendency was calculated over the equatorial central Indian Ocean (5°S–5°N, 60°–90°E) and the Indian Sub-continent and Bay of the Bengal (10°–20°N, 60°–90°E).

The column integrated MSE budget equation at intraseasonal timescales is formulated as follows:

$$\left(\frac{\partial m}{\partial t}\right)' = -\left(\boldsymbol{u}\frac{\partial m}{\partial x}\right)' - \left(\boldsymbol{v}\frac{\partial m}{\partial y}\right)' - \left(\omega\frac{\partial m}{\partial p}\right)' + \text{LHF}' + \text{SHF}' + \text{LW}' + \text{SW}' \quad (1)$$

where $\boldsymbol{u}$ represents the zonal wind vector, $\boldsymbol{v}$ the meridional wind vector, and ω the pressure velocity. LHF and SHF denote surface latent and sensible heat flux, respectively, while LW and SW represent longwave and shortwave radiative heating rates, respectively. The prime ($'$) indicates an intraseasonal (20–90-day) anomaly. The left-hand term (MSE tendency) and the first three terms on the right-hand side (MSE advection advected by wind) are vertically integrated from 1000 hPa to 100 hPa. The radiative flux terms are calculated as the differences between the top of the atmosphere and the surface.

To assess the relative contribution of eddy-eddy and eddy-mean flow interactions, we further decompose the variables in the zonal MSE advection term into a low-frequency background state (>100 day) component, a 20–90-day intraseasonal component, and a 3–10-day synoptic-scale component:

$$-\left(\boldsymbol{u}\frac{\partial m}{\partial x}\right)' = -\left(\left(\bar{u}+u'+u^*\right)\cdot\left(\frac{\partial \bar{m}}{\partial x}+\frac{\partial m'}{\partial x}+\frac{\partial m^*}{\partial x}\right)\right)' \quad (2)$$

where the overbar ($\bar{}$), a prime ($'$), and asterisk (*) denote the low-frequency, intraseasonal, and synoptic-scale components, respectively. The filtering process is conducted using a 201-point Lanczos bandpass filter [40].

2.2. Climate data analyses

The monthly SST data at a 1°×1° horizontal resolution was derived from the global sea ice and SST analyses from the Hadley Centre (HadISST version 1.1) provided by the Met Office Hadley Centre [41]. The monthly wind reanalysis data at a 2.5°×2.5° horizontal resolution was obtained from the National Centers for the Environmental Prediction–National Center for the Atmospheric Research (NCEP–NCAR) reanalysis [42]. The daily OLR data at 1.5°×1.5° horizontal resolution was obtained from the National Oceanic and Atmospheric Administration (NOAA) [43]. The daily precipitation data at a 0.5°×0.5° horizontal resolution was derived from Climate Prediction Center Global Unified Gauge-Based Analysis of Daily Precipitation [44]. The daily atmospheric variables including horizontal winds, specific humidity, shortwave radiation, longwave radiation, sensible heat flux and latent heat flux collected from the fifth-generation global atmospheric reanalysis (ERA5) produced by the European Centre for Medium-Range Weather Forecasts (ECMWF) [45], which was re-gridded to a 1.5°×1.5° horizontal resolution, were used for the MSE analysis. The ERA5 data were used considering that the reliability of the MSE budget analyses is closely related to the quality of reanalysis daily data [46,47]. The tropical cyclone data were obtained from the International Best Track Archive for Climate Stewardship (IBTrACS) version 4 from the National Centers for Environmental Information [48]. We also analyzed monthly SST and horizontal wind outputs from 28 CMIP6 models' historical simulations over the 1980–2014 period and their future simulations (the Shared Socioeconomic Pathways (SSP) 2-4.5 and SSP5-8.5) over the 2065–2099 period (Table S1 online) [49,50]. The historical simulations are forced by the present-day anthropogenic and natural forcings, whereas SSP2-4.5 by radiative forcings reaching 4.5 W/m^2 and SSP5-8.5 reaching 8.5 W/m^2.

All observational and reanalysis data cover the period 1980–2021. Anomalies were derived relative to the monthly mean climatology over the entire study period. The linear trend was calculated using the least square method to characterize the possible influence associated with global warming. To assess the climate impacts of MJO residence, precipitation days for a given grid point were defined as the days with daily precipitation amounts exceeding 0.5 mm and extreme precipitation days were defined as days with daily precipitation amounts above the 90th percentile threshold of the whole period. We also tested a 95th percentile threshold for the definition of extreme precipitation days. To analyze tropical cyclone frequency, area-averaged TC frequency at 5°× 5° degree horizontal resolution was calculated based on TC positions from the IBTrACS data. TC days were then calculated by dividing the TC frequency by four, considering that the IBTrACS data for TC position is recorded every six hours.

3. Results

3.1. Threefold increase of the MJO residence time over the Indian Ocean during Asian summer monsoon

During the Asian summer monsoon, the intraseasonal oscillation typically originates in the western tropical Indian Ocean and propagates northward/northeastward to the Indian sub-continent and the Bay of Bengal. While there has been extensive discussion on the independence of the northward and eastward propagation of convection associated with the intraseasonal oscillation during summertime [15,20], we collectively refer to them as the MJO without distinguishing between them. For example, it was found that the northward propagation associated with the boreal summer intraseasonal oscillation has a prominent eastward propagating component, which is often identified as being associated with the MJO [51,52]. We then characterize the MJO residence time over the Indian Ocean during Asian summer monsoon as the active days when the amplitude of the real-time multivariate MJO (RMM) index [38] exceeds one in its phases 1 to 3 (Fig. S1 online). Fig. 1b displays the time evolution of the June-July MJO residence time over the tropical Indian Ocean during the satellite era (1980–2020). The MJO residence time has increased at a rate of about 5.2 days per decade (exceeding the 95% significance level), consistent with a threefold increase in the residence days of MJO based on linear fitting. Sensitivity tests using different start and end years (Tables S2 online) confirm the robustness of this trend, despite minor variations in magnitude. The remarkable changes in MJO stalling behavior are further evidenced by comparing the frequency distribution as a function of MJO amplitude and phase angle (see details in the Methods) between the earliest and latest decades (1980–1999 versus 2012–2021) (Fig. S2 online). The MJO

tends to stall more frequently with increased amplitude over the Indian Ocean, especially in phases 1 and 2 (Fig. S3 online).

Considering that the MJO is an atmosphere-ocean coupled convective system, a substantial body of studies has demonstrated the importance of the background atmospheric and oceanic conditions in modulating the MJO propagation features [26,52–54]. Concomitant with the drastic increase of the MJO residence time, the tropical Indian Ocean has experienced a rapid warming [33,34]. This rapid warming is to some extent non-uniform, featuring more pronounced warming in the western than eastern tropical Indian Ocean, accompanied with an easterly wind trend at low levels [34] (Fig. 1c) and a westerly wind trend at 200 hPa (not shown). The Indian Ocean warming trend far exceeds the level of natural variability [33,34], implicating anthropogenic forcing as a significant driver [55]. We assess the effect of anthropogenic forcing on the warming pattern in 28 coupled models (Table S1 online) in historical and future warming (the Shared Socioeconomic Pathways (SSP) 2-4.5 and SSP5-8.5) simulations of the CMIP6 [49,50]. Observed patterns of SST warming and wind change in the Indian Ocean in recent decades are projected to persist in future greenhouse-gas emission scenarios (Fig. 1d, e), suggesting that anthropogenic forcing could be a substantial contributor.

The weakening of the monsoonal westerly flow and the SST warming, consistent with the response to the anthropogenic forcing, are closely associated with the increased MJO residence time over the Indian Ocean observed in recent decades (Fig. 2a). The background SST conditions favorable for the MJO stalling closely resemble the trend patterns across the tropical Indian Ocean, and the resemblance for the winds is mainly confined to the equatorial eastern tropical regions (Figs. 2a, 1c). The zonal wind anomalies related to MJO residence time shift to the Northern Hemisphere compared to the MJO-related SST anomaly signal, which could be attributed to the prevailing climatological MJO activity being predominantly located in the Northern Hemisphere during the summer season. Fig. 2a shows a scatterplot of the MJO residence time with area-averaged SST anomalies in the tropical Indian Ocean (15°S–15°N, 60°–90°E) and zonal wind anomalies over the northern tropical Indian Ocean (5°S–15°N, 80°–110°E) (Fig. 2b). The relationship between MJO residence time and background wind anomalies exhibits a strong negative correlation of up to

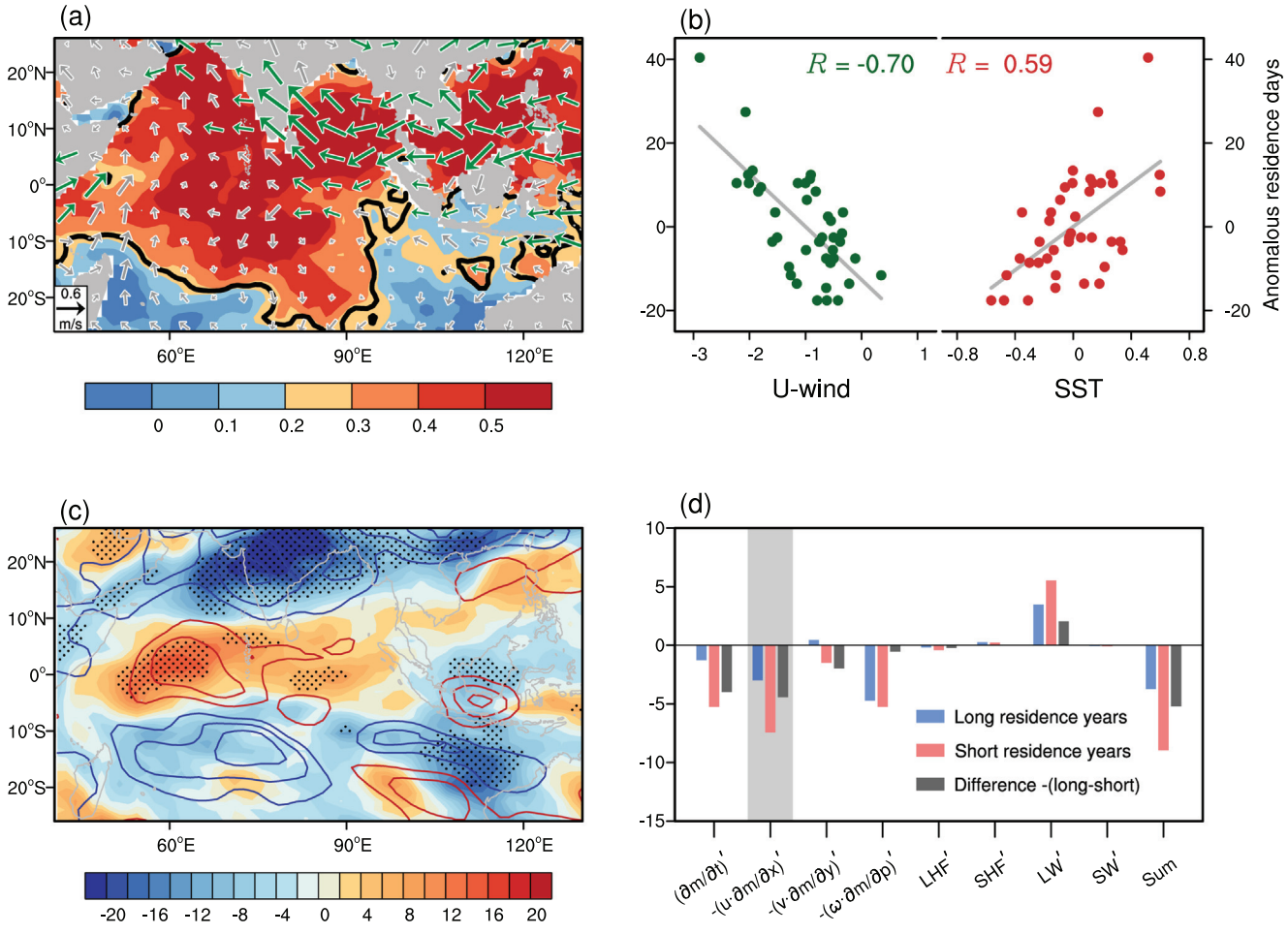


Fig. 2. Mechanisms responsible for increasing MJO residence days over the Indian Ocean in the observation. (a) Correlation of June-July averaged SST (shading; °C) and 850 hPa horizontal wind (vector; m/s) with MJO residence days over the Indian Ocean. Black lines mark correlation coefficients for SST exceeding the 90% confidence level. Correlation coefficients for winds exceeding the 90% confidence level is shown in green vectors. (b) Scatterplot of the June-July averaged MJO residence days over the Indian Ocean against 850 hPa zonal wind anomalies (green; m/s) over the northern tropical Indian Ocean (5°S–15°N, 80°–110°E) and SST anomalies (red; °C) over the tropical Indian Ocean (15°S-15°N, 60°-90°E). The linear fits (solid gray lines) are displayed together with the respective correlation coefficients (R), which are both significant at the 90% level. (c) Difference in the column-integrated moist static energy (MSE) tendency (shading; W/m^2) during MJO phases 1–3 for the years with long and short residence days (long minus short), superimposed with its long-term trend (contours; W/m^2 per 42 yr). The contour interval is 4 W/m^2 and the zero contour is omitted. The black dots represent the values significant above the 90% confidence level. (d) Area-averaged (5°S–5°N, 60°–90°E) column-integrated intraseasonal MSE budget terms (W/m^2) for the long (blue) and short (red) MJO residence years and their difference (black). From left to right, MSE tendency, zonal MSE advection, meridional MSE advection, vertical MSE advection, latent heat flux, sensible heat flux, longwave radiation, shortwave radiation, and sum of these budget terms are shown. Note that the difference (long minus short) in (d) is multiplied by a factor of –1 for illustration.

–0.70, and the correlation with background SST anomalies is 0.59. Even after removing the linear trends, the diagnosed relationship between the MJO and the basic state remains significant (Fig. S4 online), suggesting that their dynamical connection appears consistent on both interannual and longer timescales.

Despite ongoing debate over the causal relationship between background SST warming and regional wind changes [34], it is well recognized that the coupled air-sea state exerts an important impact on the local MJO-related convective activity [39,53,54]. By analyzing the MSE budget, we demonstrate that a warmer Indian Ocean and easterly wind anomalies provide persistent conditions that allow for sufficient buildup of the MJO-related convection in the Indian Ocean while simultaneously hindering its northward propagation during Asian summer monsoon (Fig. 2c). The MSE is a thermodynamic variable used to explain the propagation and maintenance of the MJO convective anomalies [25,52,56]. A positive MSE tendency generally precedes the MJO-related convection, contributing to the MJO development. Meanwhile, the MSE tendency tends to be negative at the convective center and the convection moves towards regions with positive MSE tendency. We compare the composite column-integrated intraseasonal MSE tendency during MJO phase 1–3 (Fig. S5 online) over the tropical Indian Ocean for years with long and short MJO residence times, respectively (see Methods). For short residence years (Fig. S5a online), the Indian Ocean MJO convection (phases 1–3) weakens quickly in the tropical regions, and tends to propagate towards the Indian subcontinent that experiences the largest positive MSE tendency. In contrast, during long residence years, the negative MSE tendency anomalies over the equator and positive anomalies to the north/northeast are much weakened (Fig. S5b online), setting up unfavorable conditions for the northward/northeastward propagation. The difference in the MSE tendency between long and short residence years is consistent with the long-term trend in the MSE tendency, with most (9 out of 11) years of long residence time occurring after 2000 (Fig. 2c). This suggests that MJO-related convection tends to stall over the tropical Indian Ocean where the trend of SST and MSE tendency are both positive. The favorable environment for maintaining MJO activities locally while hindering the MJO propagation is dominantly contributed by the reduced zonal MSE advection (Fig. 2d and Fig. S6 online). Specifically, the zonal MSE advection term is mainly contributed by the advection of the intraseasonal MSE anomalies by the background zonal wind ($-\bar{u}\,\partial m'/\partial x$) and the mean MSE advected by the intraseasonal zonal

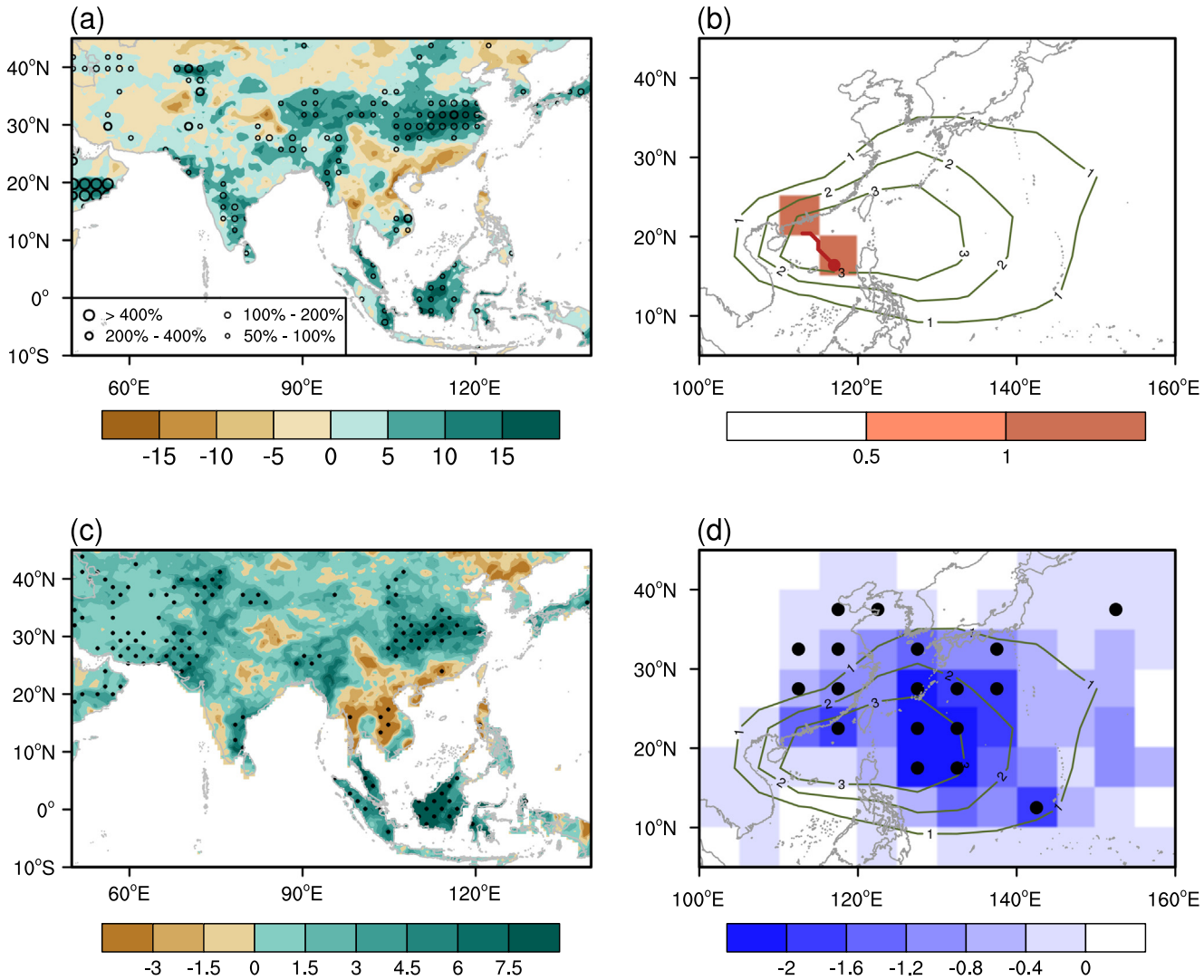


Fig. 3. Climate impacts of MJO residence over the Indian Ocean. (a) Anomalous precipitation days (shading) and the percentage of precipitation anomaly (dots; %) in June-July 2020. (b) Climatological mean (June-July) tropical cyclone days (contours) and the tropical cyclone days (shading) in June-July 2020. The red line represents the track of one tropical cyclone that occurred in June 2020. (c) Regressed precipitation days on MJO residence days during June and July with the trends removed (days per 30 days). (d) Same as (c) but for anomalous tropical cyclone days. The climatological mean (June-July) tropical cyclone days (contours) are also shown in (b) and (d) for reference. The black dots in (c) and (d) represent the significant values above the 90% confidence level.

wind anomalies ($-u'\partial\bar{m}/\partial x$) (Figs. S7 and S8 online), further emphasizing the key roles of the background wind and MSE change. While changes in the mean state MSE (Fig. S9 online) are not precisely aligned with changes in SST, they are broadly consistent considering that warmer SSTs typically correspond to a warmer and moister troposphere across a large spatial scale. Therefore, we conclude that rapid Indian Ocean warming and the low-level easterly wind trend are the main reasons for the prominent increasing trend of MJO residence time over the Indian Ocean in recent decades. Given the projected patterns of SST and wind changes (Fig. 1d, e), we expect this MJO stalling trend to continue over the 21st century.

3.2. More frequent extreme climate events linked to the increased MJO residence time

During the 2020 Asian monsoon season, MJO-related convection persisted over the tropical Indian Ocean for almost the entire June and July, and the underlying physical mechanisms driving this extreme residence are still not fully understood [27,28]. This MJO event was accompanied by unusually strong and stationary weather systems over East Asia, leading to record-breaking flooding over the plum rain belt in the past four decades (Fig. 3a) and wreaking a heavy toll on economies and ecosystems [28]. The extreme monsoon rains also doused many other parts of the Indian Ocean rim countries such as Central Asia and the Maritime Continent (Fig. 3a). Simultaneously, tropical cyclone activity was strongly suppressed over the western North Pacific with only one short-lived tropical cyclone occurring in June and an unprecedented quiescent period in July [57] (Fig. 3b). The coherence between the long-stalled MJO convection and extreme Asian monsoon rains during 2020 is more than coincidental. The close linkage between the MJO residence time and climate anomalies can be evidenced by the regression analyses on interannual timescales (Fig. 3c, d). When the MJO convection stalls over the tropical Indian Ocean, there is a tendency for more frequent wetter weather across Asian countries (Fig. 3c) and reduced cyclogenesis over the western North Pacific (Fig. 3d).

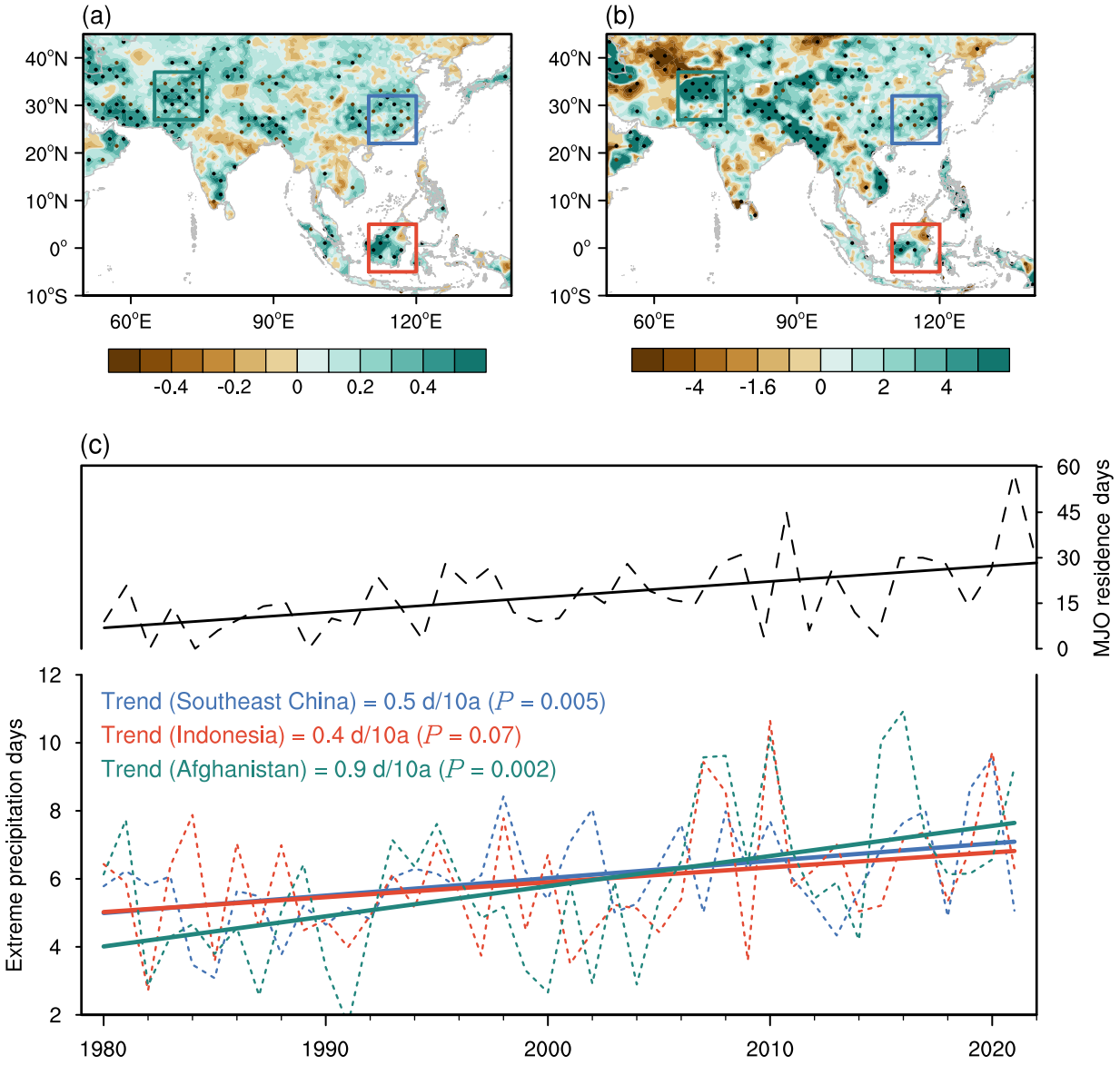


Fig. 4. Contribution of MJO residence over the Indian Ocean to more frequent extreme precipitation. (a) Regressed extreme precipitation days on MJO residence days during June and July. (b) The observed trend (days per 42 a) in the extreme precipitation days. The black dots in (a, b) represent significant values above the 90% confidence level. (c) Time series of extreme precipitation days over southeastern China (22°–32°N, 110°–120°E; blue dashed line), Indonesia (5°S–5°N, 110°–120°E; red dashed line), and Afghanistan (27°–37°N, 65°–75°E; green dashed line), superimposed by corresponding trends (solid lines) and the corresponding *P* values. The time series (gray dashed line) and trend (gray solid line) of the MJO residence time are also shown for reference.

What is particularly striking is the strong linkage between variations in MJO stalling behavior and extreme precipitation during Asian summer monsoon. We conducted a regression analysis to evaluate the impacts of the observed change in the MJO residence time over the Indian Ocean on the extreme precipitation frequency (see Methods). Fig. 4a shows that the variations in the MJO stalling days are associated with remarkably increased extreme precipitation days over Central Asia, Southeastern China, Indonesia, and the region around Nepal and Bangladesh. After excluding the possible impact from mean state change due to global warming, the relationship for these most severely affected regions remains robust (Fig. S10 online).

The regions most affected by the MJO stalling have experienced remarkable long-term rising trends of extreme precipitation frequency from 1980 to 2021 (Fig. 4b and c). For example, Central Asia, Southeastern China, and Indonesia display significant increasing trends of extreme precipitation frequency with rates rising by 0.9, 0.5, and 0.4 days per decade, respectively (Fig. 4c). Overall, the trend pattern of the extreme precipitation frequency greatly resembles that of the correlation pattern over the Asian region (Fig. 4a, b). Importantly, the results are not sensitive to the threshold of the definition of extreme precipitation days (Fig. S11 online). Considering the threefold increase in the MJO residence time over the Indian Ocean (Fig. 1b), it is natural to expect that the MJO impacts on extreme precipitation can project on the lower frequency timescales and contribute to the long-term trend of extreme precipitation days.

4. Discussion

Our analyses reveal that the MJO residence time over the Indian Ocean shows a threefold increase in the summer monsoon season from 1980 to 2021, coinciding with rapid oceanic warming and low-level easterly wind trend. There is a well-defined seasonality in the MJO stalling behavior as well as its possible long-term change along with global warming. During winter, the propagation of MJO is more regular compared to that in summer. In particular, Roxy et al. [10] demonstrate that the residence time of the MJO over the Indian Ocean shows a decreasing trend in winter, along with enhanced warming of the central Indian Ocean SST in the south and a low-level westerly wind trend at the equator (Fig. S12 online), which is consistent with the established physical connection between MJO residence time and the low-level winds.

During boreal summer, the MJO exhibits pronounced northward propagation over the Indo-Pacific warm pool with eastward propagation as clearly identified by the RMM index, although it is based on latitudinally averaged variables (Fig. S1 online). The increasing trend in summertime MJO residence time over the Indian Ocean is closely related to anomalous monsoon precipitation and, in particular strongly increased disaster risks from extreme precipitation events. It remains challenging to disentangle the direct role of the MJO in climate anomalies from its indirect effect via mean state changes in Indian Ocean SST. Nevertheless, it is important to highlight that the increasing frequency of catastrophic climate events during recent decades is directly linked to the observed MJO stalling behavior, rather than the long-term trend (Fig. 4c) or interannual climate variability. For example, Fig. S13 (online) shows that variations in precipitation days associated with the Indian Ocean SST variability (i.e., Indian Ocean basin mode) on interannual timescales are not consistent with the trend pattern of precipitation days (Fig. 4b), implying a weak direct physical connection. This suggests that changes in MJO may act as an important mediator linking Indian Ocean warming to the increasing frequency of extreme precipitation events in Asia. As Indian Ocean warming and weakened westerly winds persist as responses to anthropogenic forcing during the Asian summer monsoon season, more prolonged MJO activity over the Indian Ocean and an increase in associated extreme events in the affected regions should be anticipated.

Conflict of interest

Authors declare that they have no conflict of interest.

Acknowledgments

This work is funded by the National Key R&D Program of China (2022YFF0801602) and the US National Science Foundation (NSF) (AGS-2141728).

Author contributions

Wenjun Zhang and Fei-Fei Jin conceptualized the study; Xuben Lei, Feng Jiang, and Chao Liu led the investigation. Wenjun Zhang, Xuben Lei, and Feng Jiang wrote the manuscript. Guosen Chen, Pang-Chi Hsu, and Malte Stuecker reviewed and edited the manuscript.

Appendix A. Supplementary material

Supplementary data to this article can be found online at https://doi.org/10.1016/j.scib.2025.01.043.

References

[1] Madden RA, Julian PR. Detection of a 40–50 day oscillation in the zonal wind in the tropical Pacific. J Atmos Sci 1971;28:702–8.
[2] Ferranti L, Palmer TN, Molteni F, et al. Tropical-extratropical interaction associated with the 30–60 day oscillation and its impact on medium and extended range prediction. J Atmos Sci 1990;47:2177–99.
[3] Zhang C. Madden-Julian Oscillation: bridging weather and climate. Bull Amer Meteorol Soc 2013;94:1849–70.
[4] Stan C, Straus DM, Frederiksen JS, et al. Review of tropical-extratropical teleconnections on intraseasonal time scales. Rev Geophys 2017;55:902–37.
[5] Liebmann B, Hendon HH, Glick JD. The relationship between tropical cyclones of the western Pacific and Indian Oceans and the Madden-Julian Oscillation. J Meteorol Soc Jpn 1994;72:401–12.
[6] Camargo SJ, Wheeler MC, Sobel AH. Diagnosis of the MJO modulation of tropical cyclogenesis using an empirical index. J Geophys Res Atmos 2009;66:3061–74.
[7] Yasunari T. Cloudiness fluctuations associated with the Northern Hemisphere summer monsoon. J Meteorol Soc Jpn 1979;57:227–42.
[8] McPhaden MJ. Genesis and evolution of the 1997-98 El Niño. Science 1999;283:950–4.
[9] Guan B, Waliser DE, Molotch NP, et al. Does the Madden-Julian Oscillation influence wintertime atmospheric rivers and snowpack in the Sierra Nevada? Mon Wea Rev 2012;140:325–42.
[10] Roxy MK, Dasgupta P, McPhaden MJ, et al. Twofold expansion of the Indo-Pacific warm pool warps the MJO life cycle. Nature 2019;575:647–51.
[11] Donald A, Meinke H, Power B, et al. Near-global impact of the Madden-Julian Oscillation on rainfall. Geophys Res Lett 2006;33:2005GL025155.
[12] Jones C, Waliser DE, Lau KM, et al. Global occurrences of extreme precipitation and the Madden-Julian Oscillation: observations and predictability. J Clim 2004;17:4575–89.
[13] Matthews AJ, Hoskins BJ, Masutani M. The global response to tropical heating in the Madden-Julian Oscillation during the northern winter. Quart J Royal Meteorol Soc 2004;130:1991–2011.
[14] Wang B, Rui H. Synoptic climatology of transient tropical intraseasonal convection anomalies: 1975–1985. Meteorl Atmos Phys 1990;44:43–61.
[15] Lawrence DM, Webster PJ. The boreal summer intraseasonal oscillation: relationship between northward and eastward movement of convection. J Atmos Sci 2002;59:1593–606.
[16] Wang B, Xie X. A model for the boreal summer intraseasonal oscillation. J Atmos Sci 1997;54:72–86.
[17] Lee JY, Wang B, Wheeler MC, et al. Real-time multivariate indices for the boreal summer intraseasonal oscillation over the Asian summer monsoon region. Clim Dyn 2013;40:493–509.
[18] Annamalai H, Sperber KR. Regional heat sources and the active and break phases of boreal summer intraseasonal (30–50 day) variability. J Atmos Sci 2005;62:2726–48.
[19] Fu X, Wang B, Waliser DE, et al. Impact of atmosphere-ocean coupling on the predictability of monsoon intraseasonal oscillations. J Atmos Sci 2007;64:157–74.

[20] Chen G, Wang B. Diversity of the boreal summer intraseasonal oscillation. J Geophys Res Atmos 2021;126:e2020JD034137.
[21] Lau KM, Peng L. Origin of low-frequency (intraseasonal) oscillations in the tropical atmosphere. Part I: basic theory. J Atmos Sci 1987;44:950–72.
[22] Madden RA, Julian PR. Description of global-scale circulation cells in the tropics with a 40–50 day period. J Atmos Sci 1972;29:1109–23.
[23] Madden RA, Julian PR. Observations of the 40–50-day tropical oscillation—a review. Mon Wea Rev 1994;122:814–37.
[24] Pai DS, Bhate J, Sreejith OP, et al. Impact of MJO on the intraseasonal variation of summer monsoon rainfall over India. Clim Dyn 2011;36:41–55.
[25] Kim D, Kug JS, Sobel AH. Propagating versus nonpropagating Madden-Julian Oscillation events. J Clim 2014;27:111–25.
[26] Wang B, Chen G, Liu F. Diversity of the Madden-Julian Oscillation. Sci Adv 2019;5:eaax0220.
[27] Diamond HJ, Schreck CJ, Becker EJ, et al. The tropics. Bull Am Meteorol Soc 2021;102:S199–262.
[28] Zhang W, Huang Z, Jiang F, et al. Exceptionally persistent Madden-Julian Oscillation activity contributes to the extreme 2020 east Asian summer monsoon rainfall. Geophys Res Lett 2021;48:e2020GL091588.
[29] Wang Y, Ren H, Wei Y, et al. MJO phase swings modulate the recurring latitudinal shifts of the 2020 extreme summer-monsoon rainfall around Yangtse. J Geophys Res Atmos 2022;127:e2021JD036011.
[30] Newman M, Sardeshmukh PD, Penland C. How important is air-sea coupling in ENSO and MJO evolution? J Clim 2009;22:2958–77.
[31] Bergman JW, Hendon HH, Weickmann KM. Intraseasonal air-sea interactions at the onset of El Niño. J Clim 2001;14:1702–19.
[32] Jiang X, Waliser DE, Xavier PK, et al. Vertical structure and physical processes of the Madden-Julian Oscillation: exploring key model physics in climate simulations. J Geophys Res Atmos 2015;120:4718–48.
[33] Du Y, Xie S. Role of atmospheric adjustments in the tropical Indian Ocean warming during the 20th century in climate models. Geophys Res Lett 2008;35:2008GL033631.
[34] Roxy MK, Ritika K, Terray P, et al. The curious case of Indian Ocean warming. J Clim 2014;27:8501–9.
[35] Weller E, Min SK, Cai W, et al. Human-caused Indo-Pacific warm pool expansion. Sci Adv 2016;2:e1501719.
[36] Jones C, Carvalho LMV. Changes in the activity of the Madden-Julian Oscillation during 1958–2004. J Clim 2006;19:6353–70.
[37] Jeong JH, Kim BM, Ho CH, et al. Systematic variation in wintertime precipitation in East Asia by MJO-induced extratropical vertical motion. J Clim 2008;21:788–801.
[38] Wheeler MC, Hendon HH. An all-season real-time multivariate MJO index: development of an index for monitoring and prediction. Mon Wea Rev 2004;132:1917–32.
[39] DeMott CA, Klingaman NP, Woolnough SJ. Atmosphere-ocean coupled processes in the Madden-Julian Oscillation. Rev Geophys 2015;53:1099–154.
[40] Duchon CE. Lanczos filtering in one and two dimensions. J Appl Meteorol 1979;18:1016–22.
[41] Rayner NA. Global analyses of sea surface temperature, sea ice, and night marine air temperature since the late nineteenth century. J Geophys Res 2003;108:4407.
[42] Kalnay E, Kanamitsu M, Kistler R, et al. The NCEP/NCAR 40-year reanalysis project. Bull Amer Meteorol Soc 1996;77:437–71.
[43] Liebmann B, Smith CA. Description of a complete (interpolated) outgoing longwave radiation dataset. Bull Amer Meteorol Soc 1996;77:1275–7.
[44] Xie P, Arkin PA. Global precipitation: a 17-year monthly analysis based on gauge observations, satellite estimates, and numerical model outputs. Bull Amer Meteorol Soc 1997;78:2539–58.
[45] Hersbach H, Bell B, Berrisford P, et al. The ERA5 global reanalysis. Quart J Royal Meteoro Soc 2020;146:1999–2049.
[46] Benedict JJ, Randall DA. Observed characteristics of the MJO relative to maximum rainfall. J Atmos Sci 2007;64:2332–54.
[47] Hsu P, Li T. Role of the boundary layer moisture asymmetry in causing the eastward propagation of the Madden-Julian Oscillation. J Clim 2012;25:4914–31.
[48] Knapp KR, Kruk MC, Levinson DH, et al. The international best track archive for climate stewardship (IBTrACS): unifying tropical cyclone data. Bull Amer Meteorol Soc 2010;91:363–76.
[49] O'Neill BC, Tebaldi C, van Vuuren DP, et al. The scenario model intercomparison project (ScenarioMIP) for CMIP6. Geosci Model Dev 2016;9:3461–82.
[50] Eyring V, Bony S, Meehl GA, et al. Overview of the coupled model intercomparison project phase 6 (CMIP6) experimental design and organization. Geosci Model Dev 2016;9:1937–58.
[51] Adames ÁF, Wallace JM, Monteiro JM. Seasonality of the structure and propagation characteristics of the MJO. J Atmos Sci 2016;73:3511–26.
[52] Jiang X, Adames ÁF, Zhao M, et al. A unified moisture mode framework for seasonality of the Madden-Julian Oscillation. J Clim 2018;31:4215–24.
[53] Li Y, Han W, Wang W, et al. Intraseasonal variability of SST and precipitation in the Arabian Sea during the Indian summer monsoon: impact of ocean mixed layer depth. J Clim 2016;29:7889–910.
[54] Li Y, Han W, Wang W, et al. Bay of Bengal salinity stratification and Indian summer monsoon intraseasonal oscillation: 2. impact on SST and convection. J Geophys Res Oceans 2017;122:4312–28.
[55] Krishnan R, Sanjay J, Gnanaseelan C, et al. Assessment of Climate Change Over the Indian Region: a Report of the Ministry of Earth Sciences (MoES), Government of India. Singapore: Springer Singapore; 2020.
[56] Maloney ED. The moist static energy budget of a composite tropical intraseasonal oscillation in a climate model. J Clim 2009;22:711–29.
[57] Liu C, Zhang W, Jiang F, et al. Record-low WNP tropical cyclone activity in early summer 2020 due to Indian Ocean warming and Madden-Julian Oscillation activity. Geophys Res Lett 2021;48:e2021GL094578.